Hindawi
International Journal of Antennas and Propagation
Volume 2020, Article ID 9878607, 8 pages
https://doi.org/10.1155/2020/9878607

Research Article

Design of Low-Profile Frequency-Selective Rasorbers Based on Three-Legged Loaded Element

Yu Qiang, Dongfang Zhou, Qikun Liu, and Zhenning Yao

Department of Electromagnetic Wave and Antenna Propagation, National Digital Switching System Engineering and Technological Research Center, Zhengzhou 450002, China

Correspondence should be addressed to Yu Qiang; fisheryuzi@163.com

Received 30 October 2019; Accepted 23 December 2019; Published 9 January 2020

Academic Editor: Maggie Y. Chen

A novel low-profile dual-polarization frequency-selective rasorber (FSR) with a transmissive window in the absorption band is proposed in this paper. Based on the equivalent circuit model (ECM), the principles of the impedance design are theoretically derived. Then, a two-layer structure model is constructed. The top layer is composed of a lossy three-legged loaded element (TLLE), and the bottom layer is composed of a square ring bandpass frequency-selective surface (FSS). Furthermore, the strips are folded to reduce the unit cell size to stabilize the angular response. The maximum stable response angle increases from 20 to 40° due to the miniaturized design under both TE and TM polarization. The experimental results of the prototype are in good agreement with the simulation results, which validates the rationality of our design.

1. Introduction

Frequency-selective surface (FSS), regarded as a spatial filter within a certain bandwidth of the resonant frequency corresponding to the periodic unit cell, has been applied in hybrid radomes to transmit the in-band waves and simultaneously reflect the out-of-band waves [1]. The antenna radar cross section (RCS) could be reduced by its frequency selectivity together with a proper shape [2–4]. However, this approach is only for monostatic interrogations as the reflected waves produce lager RCSs in other directions which may still be detected by the bistatic radar system. Consequently, an ideal invisible radome should transmit the operation signals and absorb the out-of-band input power, which contributes to the generation and development of frequency-selective rasorber (FSR) technology.

Several research and applications of 2-D FSRs have been studied in the recent few years [5–16]. These FSRs are usually composed of a lossy layer and a metallic lossless bandpass FSS layer. The lossy layer can be implemented by two methods: magnetic loss material [8] and metallic element loaded with lumped resistors [5–7, 9–16]. Thus, the transmission band can be realized by the resonance of the lossy layer and the lossless layer, while the lossy layer is used to achieve absorption characteristics. Originally, the absorption band and the transmission band are separated, which results in only one-side absorption (the absorption band below the passband [5–7] and the absorption band above the passband [8–10]). To achieve a transmission window in the absorption band, some methods have been reported [11–17]. The combination of the square ring array and the crossed-dipole array realized a passband within an absorption band in [11]. Two sets of LC resonators were loaded on metal cross grids in [14]. However, in these two methods, loading too many elements leads to a complex structure. Subsequently, a 3-D FSR was constructed by using a parallel waveguide with a metallic post in the center in [17]. These structures had stable performance at the oblique incidence, but the costs of fabrication were too high.

Therefore, compared with the proposed complex structures, a more simple but stable structure by cascading a three-legged loaded element (TLLE) layer and a square ring bandpass FSS layer is proposed in this paper. This paper first elaborates the design principles of the absorption band and passband through the equivalent circuit model (ECM). The simulation results of preliminary design in the HFSS agree

well with the simulation results of the ECM in ADS. Furthermore, a miniaturized structure is proposed to improve the performance under oblique incidence. Ultimately, the prototype is fabricated and the experimental results are basically consistent with the simulation results.

2. Equivalent Circuit Analysis

According to the reported FSRs, a basic ECM usually contains three parts: a resistive layer on the top, a bandpass layer at the bottom, and an air dielectric layer in the middle. The shunt impedance between the transmission lines can be used to simulate the resistive layer and bandpass layer of the ECM.

In the absorption band of an ideal FSR, the incident waves need to be absorbed as completely as possible. That is, $|S_{11}| = 0$ and $|S_{21}| = 0$. Likewise, for the ideal passband, the insertion loss should be as low as possible. That is, $|S_{11}| = 0$ and $|S_{21}| = 1$. To achieve a transmission window in the absorption band, the operating frequencies can be divided into three regions: the lower absorption band f_{A1}, the higher absorption band f_{A2}, and the passband f_T. The relationship between three frequencies is $f_{A1} < f_T < f_{A2}$. For the absorption band f_{A1} and f_{A2}, the ECM of the resistive layer needs to realize two series resonance points, while the ECM of the bandpass layer needs to serve as the ground plane. For the passband f_T, the ECMs of the resistive layer and the bandpass layer need to realize parallel resonance at the same point. So, the equivalent circuit of the structure should have at least two series resonance points and one parallel resonance point.

Thus, an ECM that satisfies the above conditions is shown in Figure 1. Z_0 is the characteristic impendence of the free space. Z_R and Z_B represent the equivalent impendence of the resistive layer and the bandpass layer, respectively, and can be expressed as

$$Z_R = R_1 + j\omega L_1 + \frac{1}{(j\omega C_1)} + \frac{1}{[j\omega C_2 + 2/(j\omega L_2 + R_2)]},$$
$$Z_B = \frac{1}{[j\omega C_3 + 1/(j\omega L_3)]}, \tag{1}$$

where ω is the angular frequency. The resonance frequency can be computed by searching for the nulls of the derivation function of the impendence.

In the passband, L_2 and C_2, L_3 and C_3 resonate in parallel at f_T, which can be obtained as

$$f_T = \frac{1}{\left(2\pi\sqrt{L_2C_2/2}\right)} = \frac{1}{\left(2\pi\sqrt{L_3C_3}\right)}. \tag{2}$$

Thus, $Z_R \longrightarrow \infty$ and $Z_B \longrightarrow \infty$. According to [11], $|S_{11}| = 0$ and $|S_{21}| = 1$. R_2 represents the inevitable loss in the practical design, so it is set as small as possible to achieve an ideal transmission. Therefore, it is an effective method to design a structure in which the resistance layer resonates in parallel in the passband.

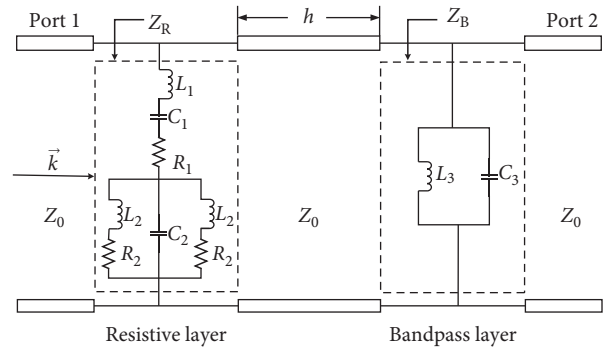

Figure 1: Equivalent circuit model.

In the absorption band, since Z_B tends to infinity at the parallel resonance frequency f_T of the bandpass layer, $Im(Z_B) = 0$ at the lower series resonant frequency f_{A1} and higher series resonant frequency f_{A2}, which can be determined by

$$f_{A1} = \frac{\sqrt{(n - \sqrt{n^2 - 8m})/2m}}{2\pi},$$
$$f_{A2} = \frac{\sqrt{(n + \sqrt{n^2 - 8m})/2m}}{2\pi}, \tag{3}$$

where

$$m = L_1L_2C_1C_2,$$
$$n = 2L_1C_1 + L_2C_2 + L_2C_1. \tag{4}$$

In conclusion, the bandpass layer performs as the ground plane when the resistive layer achieves absorption characteristics. However, it is difficult to achieve the ideal situation that all the incident waves are absorbed, so a reflection coefficient standard $|S_{11}| < -10^{\circ}$ dB is set to evaluate the absorption performance. Since the value of R_2 is very small, the real part of Z_R is mainly determined by R_1. The value of ω is related to frequency, so the value of R_1 is set near Z_0.

3. Design and Performance of the Rasorbers

3.1. Preliminary Design and Performance. A 3-D view of preliminary design based on the above ECM analysis is shown in Figure 2(a). Each unit includes a resistive layer on the top and a bandpass layer at the bottom, which are separated by air. A lossy metallic TLLE [1] and a lossless square ring bandpass FSS constitute the resistive layer and the bandpass layer, respectively, as shown in Figures 2(b) and 2(c). The lumped resistors are placed near the end of each strip in the TLLE. Both the two layers are printed on Rogers 4350B with a thickness t and a relative dielectric constant ε_r.

For the lossy metallic TLLE in the resistive layer, the two oblique strips can be decomposed into x and y directions, respectively. Then, the strips along the direction of the electric field incidence can be equivalent to a series of L_1, C_1, and R_1, while the strips perpendicular to the incident direction of the electric field can be denoted by series-parallel connection of L_2, R_2, and C_2. For the bandpass layer, the

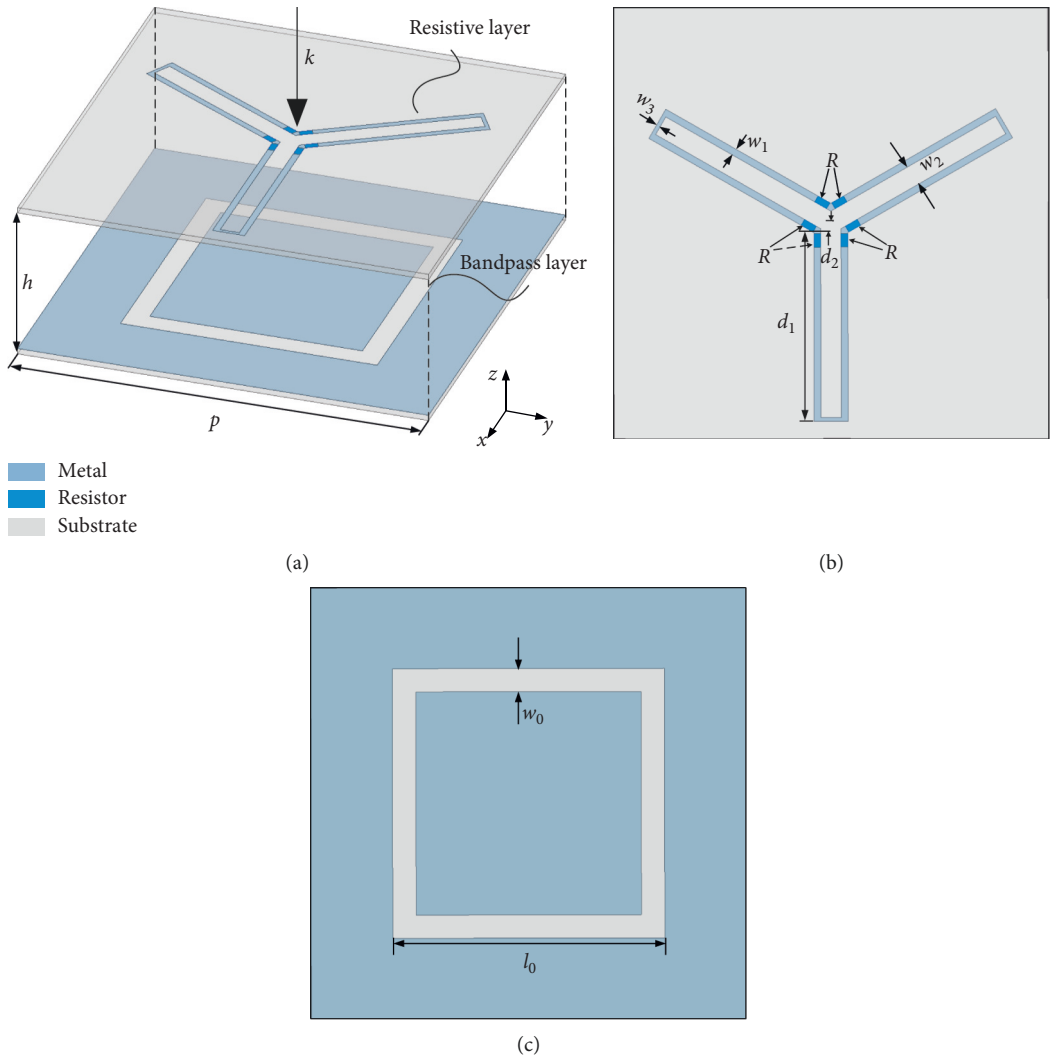

FIGURE 2: (a) 3-D view of preliminary design. (b) Resistive layer on the top. (c) Bandpass layer at the bottom (geometric dimensions: $p = 32$ mm, $h = 13$ mm, $w_1 = 0.5$ mm, $w_2 = 1.5$ mm, $w_3 = 0.29$ mm, $d_1 = 14$ mm, $d_2 = 0.8$ mm, $R = 100\,\Omega$, $w_0 = 1.72$ mm, $l_0 = 20$ mm, $t = 0.508$ mm, and $\varepsilon_r = 3.48$).

lossless square ring FSS are presented by the parallel connection of L_3 and C_3.

The reflection/transmission coefficients of the rasorber with $100\,\Omega$ and $0\,\Omega$ resistors are shown in Figure 3. By inserting resistors of $100\,\Omega$, the reflection coefficient of the absorption band drops sharply due to the ohmic loss, but the transmission coefficient of the passband is basically unaffected. Thus, it implements a transmission window within the absorption band. Moreover, to verify the effectiveness of the FSR, the surface current distributions of the TLLE at different operating frequencies are given in Figure 4. As can be seen, at f_T, the surface current density of the TLLE resistances is very small, which means that good transmission is achieved. Conversely, at f_{A1} and f_{A2}, the surface current density is very large, which means good absorption is achieved. Meanwhile, the surface current density of the resistors on each strip is different, which means that only part of the resistors in a certain absorption band mainly absorbs the incident waves.

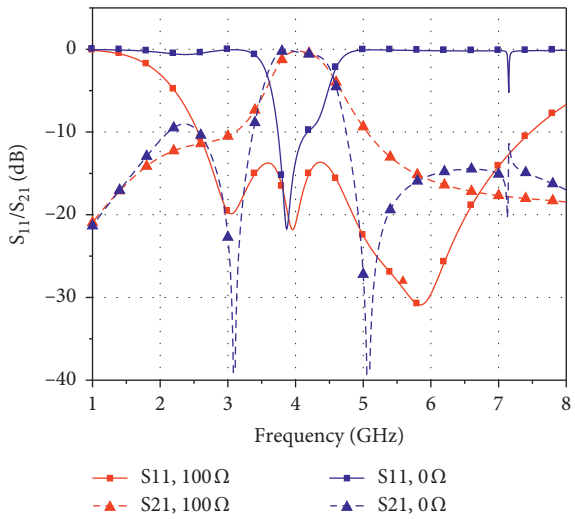

FIGURE 3: Reflection/transmission coefficients of the rasorber with $100\,\Omega$ and $0\,\Omega$ resistors.

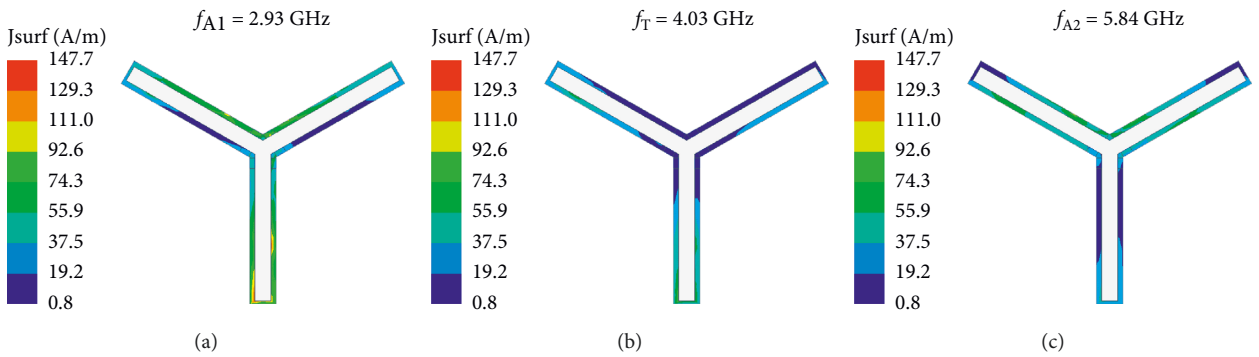

FIGURE 4: Surface current distributions of the TLLE at different operating frequencies. (a) f_{A1}: lower absorption frequency, (b) f_T: parallel resonant frequency, and (c) f_{A2}: higher absorption frequency.

The simulation results of reflection/transmission coefficients based on ECM calculations in the ADS and HFSS are shown in Figure 5. From the figure, the two curves are basically in good agreement, which further proves the rationality of our design. Different from the simulation structure in the HFSS, there is only one resistance model in the ECM, and its value is set near Z_0. Therefore, the total resistance value in HFSS simulation is larger than R_1 in ECM simulation. The slight differences in Figure 5 may be due to the loss of the dielectric substrate, which is not considered in the ECM. It is seen that the bandwidth with a reflection coefficient less than −10 dB covers 2.56 GHz to 7.47 GHz and the transmission coefficient at 4.03 GHz is only 0.24 dB under normal incidence.

In addition, the reflection/transmission coefficients at different incident angles under TE and TM polarization are studied, as shown in Figure 6. The simulation results under two polarizations are basically the same. However, as the oblique incident angle increases to 20°, the performance of the FSR deteriorates due to the generation of the grating lobe, so the model will be ameliorated to solve the problem next.

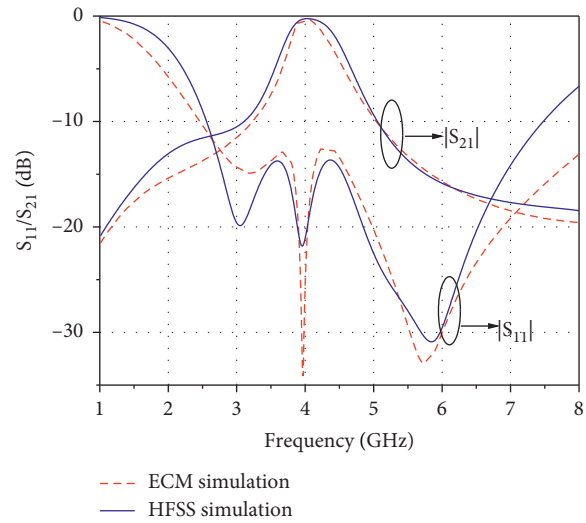

FIGURE 5: Simulation results of reflection/transmission coefficients based on ECM calculations and HFSS (circuit parameters: $L_1 = 3.81$ nH, $C_1 = 0.203$ pF, $R_1 = 390\,\Omega$, $L_2 = 5.05$ nH, $C_2 = 0.633$ pF, $R_2 = 0.5\,\Omega$, $L_3 = 2.123$ nH, $C_3 = 0.757$ pF, and $h = 13$ mm, for which the corresponding electrical length is 64° at 4.1 GHz).

3.2. Miniaturized Design and Performance. To eliminate the problem of performance degradation of the preliminary design at oblique incidence, the strips are folded to reduce the unit cell size, as shown in Figure 7. Folding strips are introduced at the bottom of the three legs, which essentially increases the electrical length of the element. Also, the bandpass FSS is replaced by the Jerusalem bandpass FSS, which has a tighter structure. Therefore, its response stability at oblique incidence is improved.

The performance of the miniaturized design under TE and TM polarization is shown in Figure 8. Under normal incidence, the insertion loss is 0.28 dB at 4.16 GHz and 0.22 dB at 4.18 GHz and the fractional width with a reflection coefficient less than −10 dB is 100.1% from 2.47 GHz to 7.5 GHz and 100.9% from 2.57 GHz to 7.8 GHz, for TE and TM polarization, respectively. The results exhibit that the miniaturized structure has a stable response with the incidence angle up to 40°, both for TE and TM polarization. Moreover, the curves have some slight fluctuations around 4.5 GHz due to harmonic resonance at oblique incidence, but anyway, it has little effect on transmission and absorption performance of the FSR.

4. Experimental Verification and Discussion

For verification, a prototype of miniaturized design is fabricated using the printed circuit board (PCB) technology, as shown in Figure 9. The prototype consists of 1×6 unit cells with a size of 22 mm × 132 mm. The unit cell dimensions follow the previous design with a periodic boundary condition. Both the resistive layer and bandpass layer are printed on a 0.508 mm thick Rogers 4350B substrate individually with a relative dielectric constant of 3.48 and a loss tangent of 0.0037. Six chip resistors (CRCW0603100RFKEAC) are soldered to the metal strips of each resistive unit cell. Two substrates are fixed by plastic screws with 13 mm thick air in the middle.

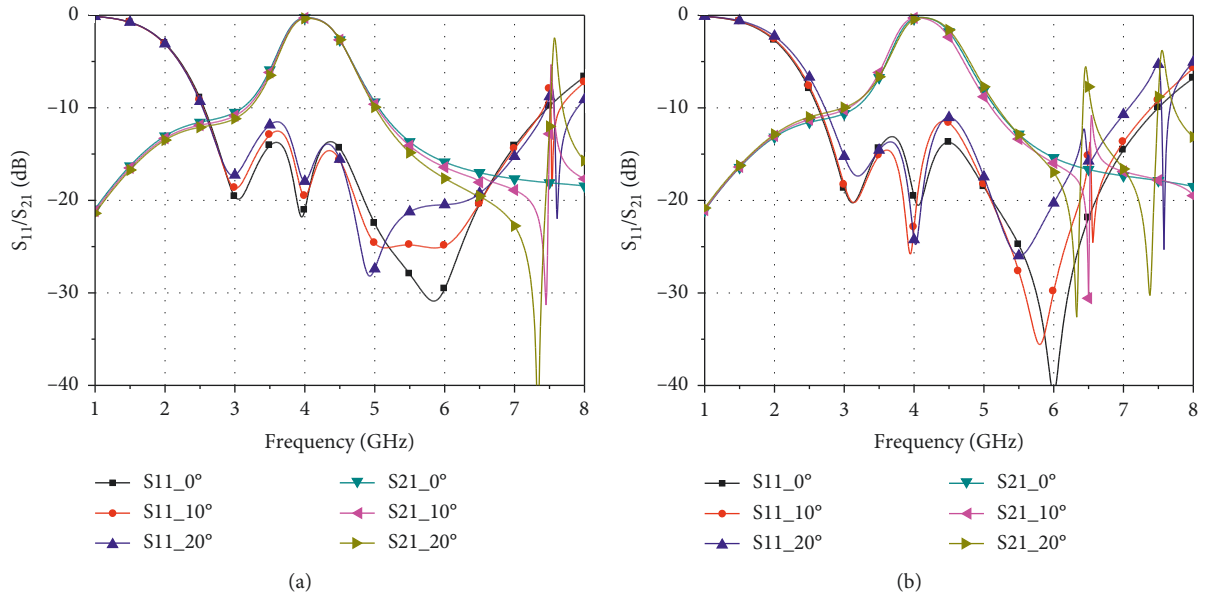

Figure 6: Simulated results of reflection/transmission coefficients of preliminary design under different oblique incidence angles. (a) TE polarization. (b) TM polarization.

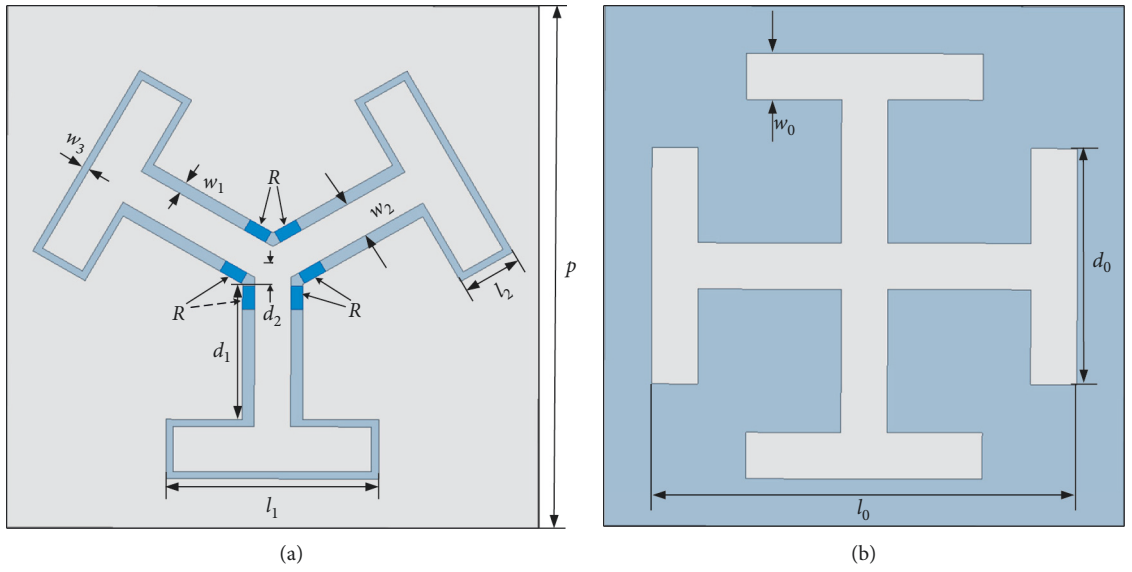

Figure 7: (a) Resistive layer on the top of the miniaturized design. (b) Bandpass layer at the bottom of the miniaturized design (geometric dimensions: $p = 22$ mm, $h = 13$ mm, $w_1 = 0.5$ mm, $w_2 = 1.5$ mm, $w_3 = 0.3$ mm, $d_1 = 6$ mm, $d_2 = 0.8$ mm, $l_1 = 8.8$ mm, $l_2 = 2.5$ mm, $R = 100\ \Omega$, $w_0 = 1.96$ mm, $l_0 = 18$ mm, $d_0 = 10$ mm).

Using a TEM cell, the sample with six unit cells is tested, which is an efficient method to characterize the periodic structures [18]. A photo of the measurement setup in a TEM cell is shown in Figure 10. An Agilent vector network analyzer (VNA) is used for the test. The tapered structures ensure that the tips of the wave top plate are connected to the input and output ports, which have subminiature type A (SMA) connectors. Measurement and simulation results under the normal incidence are shown in Figure 11. For TE polarization, the passband of the FSR sample moves to 4.32 GHz with an insertion loss of 0.73 dB and the fractional width with a reflection coefficient less than −10 dB is 99.5% from 2.65 GHz to 7.9 GHz. For TM polarization, the passband of the FSR sample moves to 4.34 GHz with an insertion loss of 0.71 dB and the fractional width with a reflection coefficient less than −10 dB is 98.2% from 2.73 GHz to 8 GHz. The differences between the simulation and measurement results may be due to the fabrication tolerance of the PCB and the inevitable loss in the test.

To better understand the performance of our design, the insertion loss of the transmission band, fractional bandwidth (FBW) of −10 dB reflection, periodicity, number of lumped

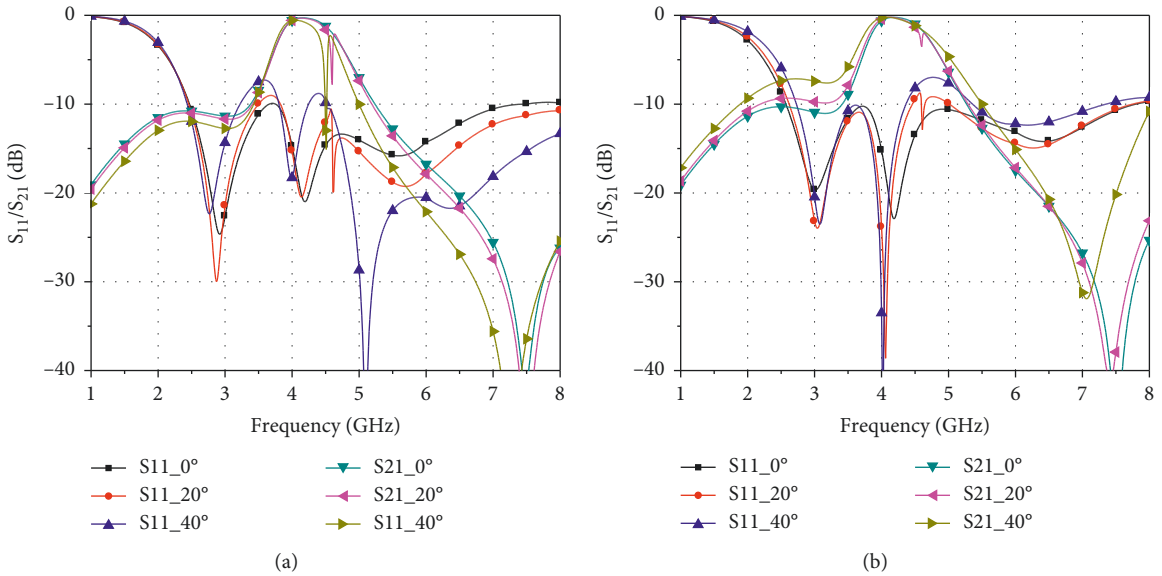

Figure 8: Simulated results of reflection/transmission coefficients of miniaturized design under different oblique incidence angles. (a) TE polarization. (b) TM polarization.

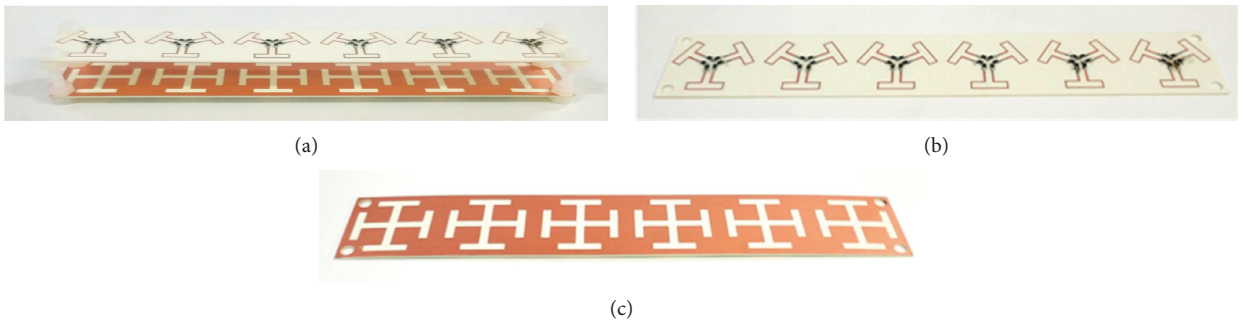

Figure 9: Photos of the fabricated rasorber. (a) Assembled structure with plastic screws. (b) Resistive layer on the top (c) Bandpass layer at the bottom.

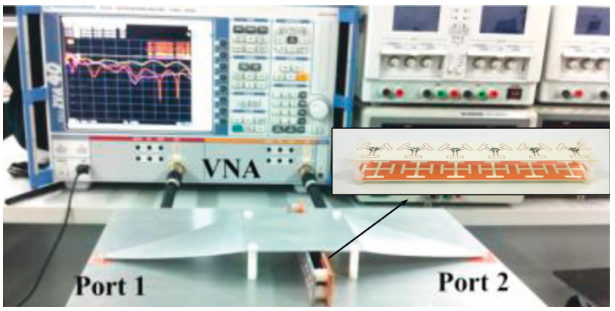

Figure 10: Photograph of the measurement setup in a TEM cell.

elements in one unit cell, and angular stability are compared with similar designs in the latest literature, as shown in Table 1. Our design, comparatively, has the lowest insertion loss in the transmission band and the least lumped elements in a unit cell, which means our rasorber has a good transmission performance and simple structure. Moreover, our rasorber has minimal periodicity except for the 3-D structure in [17], meaning a smaller profile and a more stable angular response. However, the only drawback is that the FBW of our designed rasorber is not the biggest, meaning that the absorption band is not the widest, which also needs to be further improved in the future research.

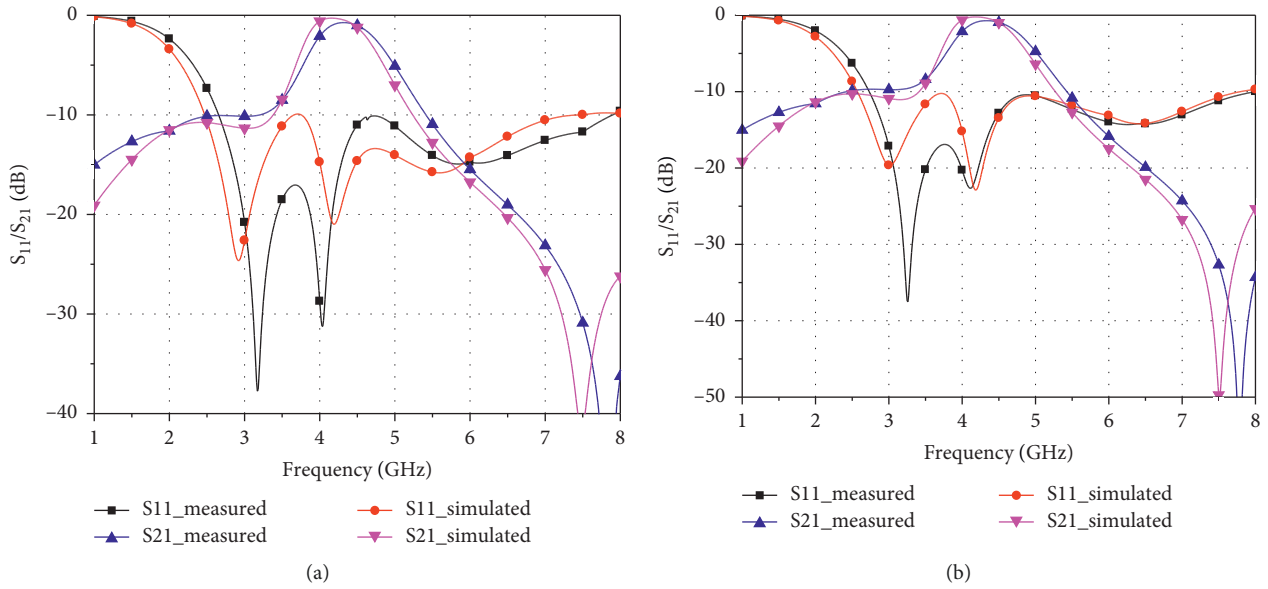

Figure 11: Measurement and simulated results under the normal incidence. (a) TE polarization. (b) TM polarization.

Table 1: Performance comparison.

Reference	Transmission band (f_T)/IL	FBW (%)	Periodicity	Number of lumped elements	Angular stability
[11]	4.42 GHz/−0.68 dB	92.3	0.37 λ_t	18	0–30°
[12]	3.54 GHz/−0.92 dB	116.9	0.3 λ_t	8	0–40°
[14]	6.62 GHz/−0.4 dB	98.8	0.44 λ_t	16	0–45°
[15]	4.25 GHz/−0.26 dB	101	0.35 λ_t	8	0–30°
[16]	10.3 GHz/−0.3 dB	108.3	0.52 λ_t	8	0–45°
[17]	2.2 GHz/−0.5 dB	114.1	0.18 λ_t	8	0–40°
This work	**4.18 GHz/−0.22 dB**	**101**	**0.31 λ_t**	**6**	**0–40°**

Ref. = reference number, IL = insertion loss, FBW = fractional bandwidth of −10 dB reflection, and λ_t = free space wavelength at the transmission frequency f_T.

5. Conclusions

A novel simple and stable low-profile rasorber with good transmissive property within a wide absorption band is proposed in this paper. The ECM is firstly analyzed which provides more insight into the FSS behavior. A lossy metallic TLLE is then chosen to implement the resistive layer, thus avoiding complex and expensive structures. Furthermore, the use of folded strips and Jerusalem structure reduces the size of the unit cell, making the angular response of the FSR more stable. Finally, the prototype is fabricated and the agreement between the measurement results and the simulation results proves the correctness of our design.

Data Availability

The data used to support the findings of this study are available from the corresponding author upon request.

Conflicts of Interest

The authors declare that there are no conflicts of interest regarding the publication of this paper.

Acknowledgments

This work was supported in part by the National Natural Science Foundation of China (grant no. 61271104).

References

[1] B. A. Munk, *Frequency Selective Surfaces*, John Wiley & Sons, Hoboken, NJ, USA, 2000.

[2] X. He, T. Chen, and X. Wang, "A novel low RCS design method for X-band vivaldi antenna," *International Journal of Antennas and Propagation*, vol. 2012, Article ID 218681, 6 pages, 2012.

[3] J. Xue, W. Jiang, and S. Gong, "Wideband RCS reduction of microstrip array antenna based on absorptive frequency selective surface and microstrip resonators," *International Journal of Antennas and Propagation*, vol. 2017, Article ID 1260973, 11 pages, 2017.

[4] E. F. Knott, J. F. Shaeffer, and M. T. Tuley, *Radar Cross Section*, SciTech Publishing, Inc., Raleigh, NC, USA, 2nd edition, 2004.

[5] X. Chen, Y. Li, Y. Fu, and N. Yuan, "Design and analysis of lumped resistor loaded metamaterial absorber with transmission band," *Optics Express*, vol. 20, no. 27, Article ID 28347, 2012.

[6] Q. Chen, S. Yang, J. Bai, and Y. Fu, "Design of absorptive/transmissive frequency-selective surface based on parallel resonance," *IEEE Transactions on Antennas and Propagation*, vol. 65, no. 9, pp. 4897–4902, 2017.

[7] Z. Wang, Q. Zeng, J. Fu et al., "A high-transmittance frequency-selective rasorber based on dipole arrays," *IEEE Access*, vol. 6, pp. 31367–31374, 2018.

[8] F. Costa and A. Monorchio, "A frequency selective radome with wideband absorbing properties," *IEEE Transactions on Antennas and Propagation*, vol. 60, no. 6, pp. 2740–2747, 2012.

[9] L.-G. Liu et al., "Design of an invisible radome by frequency selective surfaces loaded with lumped resistors," *Chinese Physics Letters*, vol. 30, no. 6, Article ID 064101, 2013.

[10] Q. Chen, J. Bai, L. Chen, and Y. Fu, "A miniaturized absorptive frequency selective surface," *IEEE Antennas and Wireless Propagation Letters*, vol. 14, no. 1, pp. 80–83, 2015.

[11] Y. Shang, Z. Shen, and S. Xiao, "Frequency-selective rasorber based on square-loop and cross-dipole arrays," *IEEE Transactions on Antennas and Propagation*, vol. 62, no. 11, pp. 5581–5589, 2014.

[12] Y. Han, W. Che, X. Xiu, W. Yang, and C. Christopoulos, "Switchable low-profile broadband frequency-selective rasorber/absorber based on slot arrays," *IEEE Transactions on Antennas and Propagation*, vol. 65, no. 12, pp. 6998–7008, 2017.

[13] H. Huang and Z. Shen, "Absorptive frequency-selective transmission structure with square-loop hybrid resonator," *IEEE Antennas and Wireless Propagation Letters*, vol. 16, pp. 3212–3215, 2017.

[14] K. Zhang, W. Jiang, and S. Gong, "Design bandpass frequency selective surface absorber using lc resonators," *IEEE Antennas and Wireless Propagation Letters*, vol. 16, pp. 2586–2589, 2017.

[15] X. Xiu, W. Che, Y. Han, and W. Yang, "Low-profile dual-polarization frequency-selective rasorbers based on simple-structure lossy cross-frame elements," *IEEE Antennas and Wireless Propagation Letters*, vol. 17, no. 6, pp. 1002–1005, 2018.

[16] Q. Chen, D. Sang, M. Guo, and Y. Fu, "Frequency-selective rasorber with interabsorption band transparent window and interdigital resonator," *IEEE Transactions on Antennas and Propagation*, vol. 66, no. 8, pp. 4105–4114, 2018.

[17] Z. Shen, J. Wang, and B. Li, "3-D frequency selective rasorber: concept, analysis, and design," *IEEE Transactions on Microwave Theory and Techniques*, vol. 64, no. 10, pp. 3087–3096, 2016.

[18] T. Nakanishi, Y. Tamayama, and M. Kitano, "Efficient second harmonic generation in a metamaterial with two resonant modes coupled through two varactor diodes," *Applied Physics Letters*, vol. 100, no. 4, Article ID 044103, 2012.